Curvilinear deflagration of energetic materials.

IGOR R. KUZNETSOV * and D. SCOTT STEWART
University of Illinois, Urbana, IL 61801, USA

November 30, 2006

Abstract

Effects of material interface curvature on deflagration of a homogeneous solid energetic material (EM) is studied in a limit when the radius of curvature is much larger than the deflagration front thickness. Under assumption of quasi-steady burning, a method of matched asymptotics is employed do derive first order curvature corrections to the mass flux across the gas/solid interface as well as to the interface temperature. As an illustration, a problem of quasi-steady spherical particle deflagration is solved numerically and the simulation results are used to verify those obtained through asymptotic analysis. An algorithm for a fully-coupled unsteady solver suitable for EM deflagration simulation is presented. Numerical solution of the unsteady spherical particle deflagration is used to show that the assumption of quasi-steady deflagration is valid.

1 INTRODUCTION

Significant effects related to material interface curvature can be observed in a variety of reacting-flow applications, and their importance in phenomena such as detonation, solidification, premixed combustion, and diffusion flames has been widely recognized. For example, the multi-dimensional dynamics and stability of flame fronts and detonations is known to be largely influenced by the correlation between the reaction front shape and its propagation velocity. This correlation is due to the change in transport to the reaction zone of the flame or detonation wave: since more heat is conducted to the concave (with respect to the fresh mixture) part of the front, the reaction rate is increased, which increases the flame speed and stabilizes the reaction front. At the same time, for premixed gas flames the change in diffusion due to curvature is destabilizing [1], so the combined effect depends on the ratio of the thermal and the mass diffusivities, or Lewis number [2]. For flames and detonations, the curvature effects are usually taken into account by modifying the planar front propagation speed [3, 4].

*Corresponding author: Igor R. Kuznetsov, Biomedical Engineering, Boston University, 44 Cummington St., Boston, MA 02215, USA (FAX: 617-353-6766, email: kouznets@bu.edu)

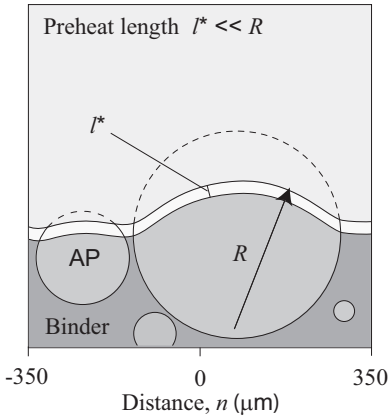

Figure 1: Propagation of a curved deflagration front through AP/HTPB composite grain.

Deflagration of EM such as solid propellants or explosives is similar in nature to the premixed gaseous flames and involves both phase transition and exothermic chemical reaction. Most of the solid propellant deflagration applications involve curved reacting surfaces, from a small-scale roughness of the granulated surface of a composite propellant to the star-shaped cross-section of a solid-propellant rocket booster grain. These facts suggest that curvature may play as important a role in solid propellant deflagration as it does in premixed flames, especially since both experiments [5] and multi-dimensional simulation [6] show that solid-propellant deflagration fronts are indeed not planar. A detailed discussion of curvature effects on the EM flame can be found in the spherical particle deflagration literature but, as we argue later, may not be directly applicable to the solid EM deflagration.

Despite its limitations, the one-dimensional approach gives predictions of measurable parameters such as the burning rate, flame stand-off distance, and surface temperature, that are in fair agreement with experimental data. This comes as no surprise since the surface radius of curvature is much larger than the deflagration zone thickness: the latter is usually of the order of a hundred micron or less, while the former is orders of magnitude larger in most solid-propellant applications. For example, under the operating conditions of a solid-rocket motor, the thermal preheat layer thickness is very small: the typical parametric values for burning of an ammonium perchlorate (AP) granule in a propellant composite (Fig. 1), in combination with the regression rate of the order of 10 mm/sec, gives an estimate of $l^* = \lambda/(C_p m_0)$ =16 μm. At the same time, the size of an AP particle can be hundreds of microns, much larger than the preheat length. Hence a planar model may be used successfully as a first-order approximation, but still the question remains of how accurate such first-order approximation is.

In order to answer this question, we find a closed-form solution to an asymp-

totic model for a general two-dimensional EM deflagration interface under the assumption that the deflagration front curvature is small compared to its thickness. A numerical simulation of the deflagration of a spherical solid propellant particle in an inert atmosphere is used to verify asymptotic solution and to illustrate how front curvature influences burning rate in a convenient computational domain geometry. Before doing that, it is worthwhile to briefly review the previous one-dimensional studies in planar and spherical geometry that are relevant to our work.

Numerous models have been proposed to describe planar deflagration, starting with the closed-form solution given by Zel'dovich [7] in 1942. Since then, various improvements have been introduced [8, 9, 10, 11, 12] to his analytical model in an attempt to capture more details of the complex physics and chemistry in condensed as well as in gas phase of the deflagrating EM (a more detailed discussion can be found in [12]). Alongside with development of analytical models, a variety of numerical approaches were suggested for EM deflagration [13, 14, 15, 16, 17]. Most of these models are formulated in one dimension and are thus limited to planar geometry.

There is a number of ways to classify existing analytical models, but for the purposes of this paper we identify two general approaches: models of deflagration controlled mostly by condensed-phase reaction rates, and those controlled mostly by gas-phase reaction rates [18]. When the condensed-phase decomposition reaction is exothermic and its activation energy is high, it is easy to derive (by using the method of matched asymptotics) a formula for the regression rate which, in turn, depends on the solid surface temperature. If the activation energy of the chemical reaction in the gas phase is also high, a similar asymptotic analysis of the gas-phase heat equation reveals another constraint for the burning-rate eigenvalue which, together with that for the solid phase, defines the burning rate and the surface temperature as unique functions of material properties, ambient pressure, and boundary conditions. This case can be viewed as intermediate between the gas-controlled and the solid-controlled deflagration, with chemical reactions in both phases defining the burning rate.

When the reaction in the gas phase has low activation energy, the gas-phase heat equation does not produce an eigenvalue, and one can say that the burning rate is controlled mostly by the condensed-phase reaction. Similarly, if the reaction in the condensed phase is omitted from the formulation and replaced with a jump in the temperature gradient at the solid–gas interface, then the gas-phase reaction solely defines the burning rate. This particular model with gas-phase controlled reaction rate is commonly used in liquid droplet combustion modeling and was adopted [19, 20] to study combustion of a mono-propellant in an inert atmosphere.

A number of authors have looked at the spherical particle surface regression rate as a function of the Damkohler number, which depends on the particle dimension. In 1969, Fendell [21] looked at the limiting cases of large and small Damkohler number and studied behavior of the surface mass flux in those limits. Using an assumption of large gas-phase activation energy, Ludford et al. [20] obtained an asymptotic solution that shows a monotonic increase in mass flux with

increasing Damkohler number. In their spherically-symmetric models, Ludford et al. solved the gas-phase equations subject to boundary conditions on the surface that imposed a jump in the temperature gradient across the interface commensurate with the heat of vaporization, while temperature inside the particle was considered to remain constant.

Recently it was suggested [11] that the effective activation energy in the gas phase may not be high in solid EM deflagration. Experimental evidence [22] for EM such as HMX suggests that the low gas-phase activation energy model produces more accurate results. This fact served as a motivation for us to revisit the formulation of particle deflagration used by Fendell [19] and to modify it for the case of condensed-phase controlled reaction.

The assumption of uniform heating of the particle interior to the melt temperature may not be accurate for the deflagration of a solid-propellant particle when the thermal preheat layer thickness is very small. Also, as seen from previous work [11], the solid-phase chemical reaction plays an important part in the determination of the regression rate, which leads us to believe that thermochemical processes in the solid phase need to be accounted for. We will consider the deflagration of a spherical mono-propellant particle in an inert atmosphere as an extension of Fendel's model including the limiting case when the chemical reaction of gaseous decomposition has low activation energy, and the surface mass flux is dictated mostly by the high activation energy reaction in the solid phase.

In what follows, we derive a burning rate eigenvalue for weakly-curved, quasi-steady deflagration of a generic EM. In Section 2, the governing equations are presented. A reduced set of the governing equations in the surface-attached intrinsic coordinates [23] is derived in Section 3, and the method of matched asymptotics is used to obtain the curvature correction to the surface regression rate and surface temperature.

A coupled gas–solid problem of spherical particle deflagration in an inert atmosphere is solved numerically and results of the calculation are compared to those obtained by asymptotic analysis in Section 4. In Section 5, the results of an unsteady deflagration calculation are used to validate the assumption of quasi-steady burning, on which our asymptotic results are based. Additional details of the unsteady simulation, and the numerical pitfalls one may encounter while applying moving interface algorithms to high activation energy reaction fronts are discussed in the Appendix 9.

2 FORMULATION

2.1 Gas Phase

The Mach number in solid-propellant combustion applications is small, therefore we use the combustion approximation [24], and expand the pressure in the gas phase as $P = p\,(t) + M^2\gamma p_1(x,t) + \ldots$. Note that the leading-order pressure term is constant throughout the entire gas-phase domain at each instant in time.

The specific heat at constant volume C_v is considered to be constant along with the thermal conductivity of the gas λ_g. The first and second viscosity coefficients are denoted μ and μ_ν, and Y is the mass fraction. The gas obeys the ideal gas law $P = \rho\mathcal{R}T/\mathcal{M}$, where ρ is density, $\mathcal{R}$ is the universal gas constant, T is temperature, and $\mathcal{M}$ is the molecular weight. A bimolecular, irreversible reaction is modeled by an Arrhenius-type term $\Omega = QBT^2\rho^2 Y \exp(-E/\mathcal{R}T)$, where B is the frequency factor and E is the gas-phase activation energy, while Q denotes the heat of reaction per unit mass.

The gas phase equations in dimensionless form, where a tilde denotes dimensional values, and the absence of tilde, nondimensional ones, are

$$\begin{aligned} \dot{\rho} &= -\rho(\vec{\nabla}\cdot\vec{v})\,, \\ \rho\dot{\vec{v}} &= -\vec{\nabla}p_1 + \mathrm{Pr}_\nu\vec{\nabla}(\vec{\nabla}\cdot\vec{v}) + \mathrm{Pr}\triangle\vec{v}\,, \\ \rho\dot{T} &= \triangle T + \Omega_g\,, \\ \rho\dot{Y} &= \frac{1}{\mathrm{Le}}\triangle Y - \Omega_g\,. \end{aligned} \tag{1}$$

Here $\vec{v}$ is material particle velocity in a laboratory frame, Y is the fuel mass fraction. The scaled ideal gas law is given by $\rho T = 1$, and the scaled reaction term is given by $\Omega_g = \mathcal{D}Y\exp(-\theta_g/T)$, where $\mathcal{D}$ is Damkohler number given by $\mathcal{D} = \tilde{\lambda}_g\tilde{B}\tilde{P}^2\tilde{\mathcal{M}}_g^2/(\tilde{m}_c^2\tilde{\mathcal{R}}^2\tilde{C}_p)$.

The gas phase scales used (denoted here by subscript c) are: mass flux scale $\tilde{m}_c$, pressure scale $\tilde{P}_c = \tilde{P}$, density scale $\tilde{\rho}_c^g = \tilde{P}_c\tilde{\mathcal{M}}_g/(\tilde{T}_c^g\tilde{\mathcal{R}})$, temperature scale $\tilde{T}_c^g = \tilde{Q}_g/\tilde{C}_p$, velocity scale $\tilde{v}_c = \tilde{m}_c/\tilde{\rho}_c^g$, length scale $\tilde{l}_c^g = \tilde{\lambda}_g/(\tilde{C}_p\tilde{m}_c)$, and time scale $\tilde{t}_c^g = \tilde{l}_c^g/\tilde{v}_c$. Also, we define Lewis number $Le = \tilde{d}\tilde{C}_p/\tilde{\lambda}_g$, where $\tilde{d}$ is the diffusion coefficient. Mach number is given by $M^2 = \tilde{v}_c^2\tilde{\mathcal{M}}_g/(\gamma\tilde{\mathcal{R}}\tilde{T}_c^g)$, and activation energy in the gas phase is given by $\theta_g = \tilde{E}_g\tilde{C}_p/(\tilde{\mathcal{R}}\tilde{Q}_g)$. Prandtl numbers are defined as $Pr = \tilde{\mu}\tilde{C}_p/\tilde{\lambda}_g$ and $Pr_\nu = \tilde{\mu}_\nu\tilde{C}_p/\tilde{\lambda}_g$, specific heat ratio is $\gamma = \tilde{C}_p/\tilde{C}_v$. In the above, $\tilde{C}_p$ is the specific heat at constant pressure.

2.2 Solid Phase

The solid phase is treated as a reacting, incompressible conducting material (similar formulation for a more general reacting thermoelastic solid with thermal expansion can be found in [25]). The formulation will be restricted to the energy conservation equation for brevity, and is sufficient for the following analysis:

$$\rho\dot{T} = \triangle T + \Omega_s\,. \tag{2}$$

The unimolecular, irreversible, zeroth-order solid-phase reaction is modeled by an Arrhenius-type term $\Omega_s = A\exp(-\theta_s/T)$. The frequency factor A and the activation energy θ_s are defined as $A = \tilde{\lambda}_s\tilde{\rho}_s\tilde{Z}/(\tilde{m}_c^2\tilde{C}_p)$, $\theta_s = \tilde{E}_s\tilde{C}_p/(\tilde{\mathcal{R}}\tilde{Q}_s)$, where $\tilde{E}_s$ is the activation energy. The thermal conductivity $\tilde{\lambda}_s$ is constant, and the specific heat of the solid phase is set equal to that of the gas phase. The solid-phase scales used are: mass flux scale $\tilde{m}_c$, density scale $\tilde{\rho}_c^s$, temperature scale $\tilde{T}_c^s = \tilde{Q}_s/\tilde{C}_p$, length scale $\tilde{l}_c^s = \tilde{\lambda}_s/(\tilde{C}_p\tilde{m}_c)$, and time scale $\tilde{t}_c^s = \tilde{l}_c^s\tilde{\rho}_c^s/\tilde{m}_c$.

3 QUASISTEADY SP FLAME STRUCTURE

3.1 Surface-Attached Coordinates

In the following analysis we resort to the coordinates aligned with the curves that are, at each point of space and time, parallel and normal to the propellant surface. A similar approach was adopted for the study of slightly curved detonation fronts in [4]. The formulation is restricted to two dimensions for brevity. These Bertrand-intrinsic coordinates are related to the laboratory coordinates through the transformation rule

$$\vec{x} = \vec{x}_s(\xi, t) + n\,\hat{n}(\xi, t)\,, \tag{3}$$

where $\vec{x} = \vec{x}_s(x, y, t)$ are the laboratory frame position vectors of the points on the surface of the burning material $\psi(x, y, t) = 0$, which can also be parametrized by the length along the coordinate line on the surface ξ at time t as $\vec{x} = \vec{x}_s(\xi, t)$. The unit normal and tangent vectors are given by $\hat{n} = \vec{\nabla}\psi/|\vec{\nabla}\psi|$ and $\hat{t} = \partial\vec{x}_s/\partial\xi$, correspondingly. The position of each point in space in Bertrand coordinates is given by the variables n and ξ, which are the normal distance from the surface and the arc length along the principal lines of curvature of the surface. The surface curvature is defined by $\kappa(\xi, t) = \vec{\nabla} \cdot \hat{n}$. With the help of the transformation rule (3), the governing equations are rewritten in the intrinsic coordinates. The transformed system of equations can be found in Appendix 7.

3.2 Governing equations with curvature correction

Under the assumption of small curvature κ, the variation of the flow in the tangential direction is weak in both gas and solid phases. Based on this fact, we write out a reduced system of equations (Appendix 8) that is accurate to $O(\kappa)$. For the gas phase, the system of reduced equations is

$$\frac{\mathrm{d}}{\mathrm{d}n}\left(\rho U_n\right) = -\kappa\rho(U_n + D)\,, \tag{4}$$

$$\frac{\mathrm{d}}{\mathrm{d}n}\left[\rho U_n^2 + p_1 - \mathrm{Pr}^*\frac{\mathrm{dU_n}}{\mathrm{dn}}\right] = -\kappa\left[\rho U_n(U_n + D) - \mathrm{Pr}^*\frac{\mathrm{d^2U_n}}{\mathrm{dn^2}}\right], \tag{5}$$

$$\frac{\mathrm{d}}{\mathrm{d}n}\left[\rho U_n(T + Y) - \frac{\mathrm{d}H}{\mathrm{d}n}\right] = -\kappa\left[\rho(U_n + D)(T + Y) - \frac{\mathrm{d}H}{\mathrm{d}n}\right], \tag{6}$$

$$\rho U_n\frac{\mathrm{d}T}{\mathrm{d}n} - \frac{\mathrm{d}^2T}{\mathrm{d}n^2} - \mathcal{D}Y\exp\left(-\frac{\theta_g}{T}\right) = \kappa\frac{\mathrm{d}T}{\mathrm{d}n}\,, \tag{7}$$

where U_n is the particle velocity in the moving frame, $\mathcal{D}$ is the Damkohler number, $\mathrm{Pr}^* = \mathrm{Pr} + \mathrm{Pr}_\nu$, and $H = T + Y/\mathrm{Le}$. The time derivatives are absent due to the quasi-steady character of the deflagration process in the limit of small surface curvature and the fact that the flow parameters change on a much smaller time scale than the domain geometry. In this quasi-steady formulation, the geometry is fixed and the flow in the attached intrinsic frame is steady. As

we can see, the system of equations for the gas phase has reduced to a system of one-dimensional conservation equations for the planar combustion with the addition of the curvature correction terms.

In a similar way, we deduce for the solid phase:

$$\frac{\mathrm{d}}{\mathrm{d}n}\left(\rho U_n T - \frac{dT}{dn}\right) - \Omega_s = \kappa\left[\frac{\mathrm{d}T}{\mathrm{d}n} - \rho(U_n + D)T\right]. \tag{8}$$

3.3 Interface Jump Conditions

To ensure that fluxes are continuous at the interface separating solid and gas phases (defined as a point where the solid-phase reaction is complete), the governing equations are supplemented with boundary conditions as follows:

$$[\rho U_n] = 0\,, \quad [T] = 0\,, \quad \left[\lambda\frac{\mathrm{d}T}{\mathrm{d}n}\right] = 0\,, \quad Y(0) - \frac{1}{m_s}\frac{\mathrm{d}Y(0)}{\mathrm{d}n} = 1\,. \tag{9}$$

Here square brackets represent the jump in the quantity inside the brackets across the solid–gas interface, and m_s is the mass flux at the interface.

3.4 Burning Rate Eigenvalue with Curvature Correction

The mass flux correction is derived in two steps. First, we look at the condensed phase thermal structure and, holding the curvature as a finite parameter, use large activation energy asymptotics to derive the relationship between the curvature-corrected mass flux eigenvalue and the surface temperature. The second step involves a similar asymptotic analysis of the gas phase thermal structure and matching the gas-phase and solid-phase solutions at the interface in order to obtain unique values of the surface temperature and mass flux corrections as functions of material properties and boundary conditions.

3.4.1 Solid phase thermomechanical structure asymptotics

Since we choose to model the solid phase as incompressible, the material particles in the condensed phase are at rest with respect to the laboratory frame. The material velocity in the moving frame U_n is a negative of the interface velocity D: $U_n + D \equiv u_n = 0$. The energy equation in the solid phase reduces to

$$\frac{\mathrm{d}T}{\mathrm{d}n}(m_s - \kappa) = \frac{\mathrm{d}^2T}{\mathrm{d}n^2} + \Lambda\theta_s \exp\left(\frac{\theta_s}{T_s} - \frac{\theta_s}{T}\right), \tag{10}$$

with boundary conditions $T(0) = T_s$ and $T(-\infty) = T_0$, and $\mathrm{d}T(-\infty)/\mathrm{d}n = 0$. Here T_s and $m_s = \rho_s U_n > 0$ are the surface temperature and mass flux with correction for curvature. The reduced Damkohler number Λ and activation energy θ_s are defined as

$$\Lambda = A\theta\exp(-\theta_s/T_s)\,, \quad \theta_s = \tilde{E}_s\tilde{C}_p/(\tilde{\mathcal{R}}\tilde{Q}_s)\,, \quad A = \tilde{\lambda}_s\tilde{\rho}_s\tilde{Z}/(\tilde{m}_c^2\tilde{C}_p)\,. \tag{11}$$

At this point, we treat the curvature as a finite parameter and look for the mass flux eigenvalue of equation (10). In the limit of large activation energy θ_s, we show that, in order to satisfy the boundary condition, the mass flux m has to be a single-valued function of the surface temperature T_s. In that limit, the condensed phase reaction is bounded to a narrow region near the material interface, which we will call the inner region. Far from this interface, or in the outer region, the chemical reaction term is exponentially small. Matching the inner and outer region solutions, the constraint for the mass flux is deduced as follows.

Based on the assumption of a near-surface boundary layer, we introduce the layer coordinate $s = n\,\theta_s$, and look for the inner solution in the form

$$T_{\rm inner}(s) = T_s + \frac{1}{\theta_s} t^{(1)}(s) + \dots \,. \tag{12}$$

In this layer, diffusion is a dominant effect, and advection is uniformly small. The inner-layer heat equation becomes

$$\frac{{\rm d}^2 t^{(1)}}{{\rm d}s^2} + \Lambda \exp\left(\frac{t^{(1)}}{T_s^2}\right) = 0\,, \tag{13}$$

subject to the boundary condition $t^{(1)}(0) = 0$, since the surface temperature is prescribed at $s = 0$. The other boundary condition for Eq. (13) is found from matching the inner reaction layer with the outer preheat layer.

The outer solution is in the form

$$T_{\rm outer}(n) = T^{(0)}(n) + \frac{1}{\theta_s} T^{(1)}(n) + \dots \,. \tag{14}$$

Since the reaction term is exponentially small away from the reaction zone, we obtain

$$\frac{{\rm d}T^{(0)}}{{\rm d}n}(m_s - \kappa) = \frac{{\rm d}^2 T^{(0)}}{{\rm d}n^2}, \qquad T^{(0)}(0) = T_s, \qquad T^{(0)}(-\infty) = T_0\,, \tag{15}$$

$$\frac{{\rm d}T^{(1)}}{{\rm d}n}(m_s - \kappa) = \frac{{\rm d}^2 T^{(1)}}{{\rm d}n^2}, \qquad T^{(1)}(-\infty) = 0\,, \tag{16}$$

which generates a two-term outer expansion

$$T_{\rm outer}(n) = T_0 + (T_s - T_0)\exp\left[(m_s - \kappa)n\right] + \frac{1}{\theta_s} B \exp\left[(m_s - \kappa)n\right] + \dots \,. \tag{17}$$

The two-term outer-layer solution expanded for small n and written in terms of inner variable becomes

$$T_{\rm outer}(s) = 1 + \frac{1}{\theta_s}\left[B + s(m_s - \kappa)(T_s - T_0)\right] + O(\frac{1}{\theta_s})\,. \tag{18}$$

Matching gives the condition

$$\lim_{s\to-\infty} t^{(1)}(s) = s(m_s - \kappa)(T_s - T_0) + O(1)\,. \tag{19}$$

The regression eigenvalue is found in a standard way by multiplying the reaction-zone equation (13) by $\mathrm{d}t^{(1)}/\mathrm{d}s$ and integrating over the interval $(-\infty, 0]$ to obtain

$$\Lambda = \left[(\mathrm{d}t^{(1)}/\mathrm{d}s(-\infty))^2 - (\mathrm{d}t^{(1)}/\mathrm{d}s(0))^2 \right] / (2T_s) \, .$$

Matching shows that $\mathrm{d}t^{(1)}(0)/\mathrm{d}s = \mathrm{d}T(0)/\mathrm{d}n$. The temperature gradient at the surface can be calculated from a global energy balance in the solid propellant by integrating equation (10) over the thermal structure to obtain

$$\frac{\mathrm{d}T(0)}{\mathrm{d}n} = (T_s - T_0)(m_s - \kappa) - m_s \, . \tag{20}$$

From (19), one finds $\mathrm{d}t^{(1)}(-\infty)/\mathrm{d}s = (T_s - T_0)(m_s - \kappa)$ so that the formula for Λ becomes

$$\Lambda = m_s T_s^{-2} \left[(T_s - T_0)(m_s - \kappa) - \frac{m_s}{2} \right] \, . \tag{21}$$

Solving quadratic equation, we obtain:

$$m_s = \frac{\kappa(T_s - T_0) + \sqrt{\kappa^2 (T_s - T_0)^2 + 4\Lambda (T_s - T_0 - 1/2) T_s^2}}{2(T_s - T_0) - 1} \, . \tag{22}$$

This expression establishes a relationship between the burning rate (in terms of the mass flux m_s) of the curved material interface and the surface temperature T_s. It can be viewed as a generalization of the similar one-dimensional high activation energy result obtained by Merzhanov [8] to multi-dimensions in the limit when the deflagration front radius of curvature is large compared with the deflagration front thickness. If curvature κ in (22) is set equal to zero, the classical Merzhanov's mass flux formula is obtained.

Next take the limit of small curvature, and assume that the radius of curvature is large enough so that $\kappa \, \theta_s \ll 1$. This assumption is justified for typical solid EM because the value of θ_s is usually of the order $O(10)$, while the radius of curvature of the burning surface scaled with respect to the preheat length can be arbitrarily large.

Substituting a formal expansion of the surface mass flux in curvature $m_s = m_s^{(0)} + \kappa m_s^{(2)} + O(\kappa^2)$, as well as that of the surface temperature $T_s = T_s^{(0)} + \kappa T_s^{(2)} + O(\kappa^2)$, we expand (22) in powers of κ. At the first order, we obtain familiar Merzhanov's formula

$$(m_s^{(0)})^2 = \frac{A(T^* + T_0)^2 \exp\left(-\theta_s/(T^* + T_0)\right)}{\theta_s \, (T^* - 1/2)} \, , \tag{23}$$

where $T^* = T_s^{(0)} - T_0$ is introduced for convenience of presentation. At the next order, we find the curvature correction for the mass flux as

$$m_s^{(2)} = T_s^{(2)} m_s^{(0)} \left[\frac{1}{T^* + T_0} + \frac{\theta_s}{2(T^* + T_0)^2} - \frac{1}{2T^* - 1} \right] + \frac{T^*}{2T^* - 1} \, . \tag{24}$$

Expressions (23) and (24) define the planar mass flux and its curvature corrections as functions of surface temperature. In order to define the burn rate and surface temperature uniquely, we need to solve coupled gas- and solid-phase equations with appropriate boundary conditions. The matching of the temperature profiles at the burning interface will provide additional condition for planar problem, as well as for the curvature corrections, allowing to determine explicit expressions for values of temperature and regression rate.

3.4.2 Gas phase thermomechanical structure asymptotics

To determine the curvature correction to the surface temperature, we expand equations (5) in powers of curvature κ. We also assume that $Le = 1$ which simplifies the variable H defined earlier so that it becomes $H = T + Y$. The model of zero gas-phase activation energy [11] is invoked. In the limit of small gas phase activation energy, at first order in curvature we retrieve the planar deflagration equations:

$$\frac{\mathrm{d}}{\mathrm{d}n}\left(m^{(0)}\right) = 0\,, \tag{25}$$

$$\frac{\mathrm{d}}{\mathrm{d}n}\left[m^{(0)}U_n^{(0)} + p_1^{(0)} - \mathrm{Pr}^*\frac{\mathrm{dU_n^{(0)}}}{\mathrm{dn}}\right] = 0\,, \tag{26}$$

$$\frac{\mathrm{d}}{\mathrm{d}n}\left(m^{(0)}H^{(0)} - \frac{\mathrm{d}H^{(0)}}{\mathrm{d}n}\right) = 0\,, \tag{27}$$

$$\frac{\mathrm{d}}{\mathrm{d}n}\left(m^{(0)}T^{(0)} - \frac{\mathrm{d}T^{(0)}}{\mathrm{d}n}\right) = \mathcal{D}(H^{(0)} - T^{(0)})\,. \tag{28}$$

Solution of (25) shows that the planar mass flux is a constant: $m^{(0)} = m_s^{(0)}$. Equation (27) yields $H^{(0)} = H^{(0)}(\infty) = T_\infty^{(0)}$, where the adiabatic flame temperature is defined from global energy balance as $T_\infty^{(0)} = T_0 + Q^* + 1$. Now (28) can be expressed in terms of temperature only and solved, with boundary conditions $T^{(0)}(0) = T_s^{(0)}$, $T^{(0)}(\infty) = T_\infty^{(0)}$, yielding

$$T^{(0)} = T_\infty^{(0)} + (T_s^{(0)} - T_\infty^{(0)})e^{\alpha n}\,, \quad \alpha = \frac{m_s^{(0)} - \sqrt{4\mathcal{D} + (m_s^{(0)})^2}}{2}\,. \tag{29}$$

The coupled system of the planar deflagration equations is closed through matching of the temperature gradients at the interface, and unique values of the surface temperature and mass flux are obtained [11] by solving an algebraic equation

$$T^* = Q^* + \frac{1}{x_g m_s^{(0)} + 1}\,. \tag{30}$$

Here $Q^* = Q_s/Q_g$, and $x_g = 2/(\sqrt{(m_s^{(0)})^2 + 4\mathcal{D}} - m_s^{(0)})$. The planar mass flux

$m_s^{(0)}$ is defined by expression (23), recast for the gas phase scaled quantities as

$$(m_s^{(0)})^2 = \frac{A(T^*+T_0)^2 \exp\left(-\theta_s Q^*/(T^*+T_0)\right)}{Q^*\theta_s\left(T^*-Q^*/2\right)}\,. \tag{31}$$

While the boundary conditions for the zeroth order problem were those of the planar deflagration, at the next order the boundary conditions at infinity are, in general, not defined. The limit of small curvature and formulation in the intrinsic coordinates is valid for distances that are small compared to the radius of curvature, namely the condition $n\kappa \ll 1$ must be satisfied. For distances greater that that, an "outer" solution would have to be constructed. Depending on the flow configuration, such outer solution would present specific boundary condition for $n \to \infty$ of the "inner" solution in the intrinsic coordinates. For example, for a burning solid propellant particle, the outer flow far away from the surface would be a flow from a point source, while the outer solution for the infinite half-plane with uneven surface would be planar. For now, we are going to leave the outer boundary conditions in a general form and work out the inner solution keeping in mind that at infinity we have to be able to match it with the 'arbitrary' outer solution.

At the next order $O(\kappa)$, equations (5) yield

$$m^{(2)} = B_1 - \mathcal{I}_1\,, \tag{32}$$

$$m_s^{(0)}U_n^{(2)} + m^{(2)}U_n^{(0)} + p_1^{(2)} - \mathrm{Pr}^*\frac{\mathrm{d}U_n^{(2)}}{\mathrm{d}n} = B_2 - \mathcal{I}_2\,, \tag{33}$$

$$m^{(2)}H^{(0)} + m_s^{(0)}H^{(2)} - \frac{\mathrm{d}H^{(2)}}{\mathrm{d}n} = B_3 - \mathcal{I}_3\,, \tag{34}$$

$$m^{(2)}\frac{\mathrm{d}T^{(0)}}{\mathrm{d}n} + m_s^{(0)}\frac{\mathrm{d}T^{(2)}}{\mathrm{d}n} - \frac{\mathrm{d}^2T^{(2)}}{\mathrm{d}n^2} = \frac{\mathrm{d}T^{(0)}}{\mathrm{d}n} + \mathcal{D}\left(H^{(2)} - T^{(2)}\right) \tag{35}$$

where B_1, B_2, and B_3 are constants of integration, and the integrals $\mathcal{I}_i$ are defined as

$$\mathcal{I}_1 = \int_0^n \left[m_s^{(0)} + \rho^{(0)}D^{(0)}\right]\mathrm{d}n\,, \quad \mathcal{I}_2 = \int_0^n \left[m_s^{(0)}(U_n^{(0)} + D^{(0)}) - \mathrm{Pr}^*\frac{d^2U_n^{(0)}}{dn^2}\right]\mathrm{d}n\,,$$

$$\mathcal{I}_3 = \int_0^n \left[(m_s^{(0)} + \rho^{(0)}D^{(0)})H^{(0)} - \frac{\mathrm{d}H^{(0)}}{\mathrm{d}n}\right]\mathrm{d}n\,.$$

In order to solve the energy conservation equation (35), we need to express $m^{(2)}$ and $H^{(2)}$ in terms of temperature. Recalling that $H^{(0)} = T_s^{(0)} + Y_s^{(0)}$, we solve (32) and (34) for $H^{(2)}$. In order for $H^{(2)}$ to be matched to the outer solution, we set the constant multiplying the exponentially growing term to zero, which leads to $H^{(2)}(n) = H^{(2)}(\infty)$. Since $H^{(2)} = Y^{(2)} + T^{(2)}$, we obtain $\mathrm{d}Y_s^{(2)}/\mathrm{d}n + \mathrm{d}T_s^{(2)}/\mathrm{d}n = 0$ which can be substituted in the curvature expansion of the third jump condition (9) to obtain $m_s^{(0)}Y_s^{(2)} = m_s^{(2)}(T_s^{(0)} - T_\infty^{(0)} + 1) -$

$\mathrm{d}T_s^{(2)}/\mathrm{d}n$. Taking into account that planar adiabatic flame temperature is given by $T_\infty^{(0)} = T_0^{(0)} + Q^* + 1$, we finally arrive at

$$m_s^{(0)} H^{(2)} = m_s^{(0)} T_s^{(2)} - m_s^{(2)} (Q^* - T^*) - \frac{\mathrm{d}T_s^{(2)}}{\mathrm{d}n} \,. \tag{36}$$

The left hand side of (35) contains $m^{(2)}$, which can be expressed as an explicit function of coordinate n. In order to do that, we integrate (32) using $P = \rho^{(0)} T^{(0)}$, where $T^{(0)}$ is given by (29), and keeping in mind that $D^{(0)} = m_s^{(0)}/\rho_s$, where ρ_s is the solid phase density. Finally, we obtain

$$m^{(2)} = m_s^{(2)} - m_s^{(0)} \left(1 + \frac{1}{T_\infty^{(0)} \rho_s} \right) n + \frac{D^{(0)}}{\alpha T_\infty^{(0)}} \log \left[1 + \left(\frac{T_s^{(0)}}{T_\infty^{(0)}} - 1 \right) e^{\alpha n} \right] . \tag{37}$$

Now equation (35) can be rewritten as a linear ODE with known functions given by (36) and (37) on the right hand side:

$$\frac{\mathrm{d}^2 T^{(2)}}{\mathrm{d}n^2} - m_s^{(0)} \frac{\mathrm{d}T^{(2)}}{\mathrm{d}n} + \mathcal{D} T^{(2)} = \frac{\mathrm{d}T^{(0)}}{\mathrm{d}n} \left(m^{(2)} - 1 \right) - \mathcal{D} H^{(2)} \,. \tag{38}$$

We are interested in the solution to this equation at $n = 0$, since our purpose is to determine temperature correction $T^{(2)}(0)$. We find the general form of the solution to the above linear differential equation by a variational method [26] and evaluate the solution at $n = 0$. The general solution is given by

$$T^{(2)} = C_1(n) e^{\alpha n} + C_2(n) e^{\beta n} \,, \tag{39}$$

where

$$\alpha = \frac{1}{2} \left[m_s^{(0)} - \sqrt{\left(m_s^{(0)} \right)^2 + 4\mathcal{D}} \right] , \quad \beta = \frac{1}{2} \left[m_s^{(0)} + \sqrt{\left(m_s^{(0)} \right)^2 + 4\mathcal{D}} \right] , \tag{40}$$

with functions C_1 and C_2 determined from equations

$$\frac{\mathrm{d}C_1}{\mathrm{d}n} = e^{-\alpha n} \frac{f(n)}{\alpha - \beta} \,, \quad \frac{\mathrm{d}C_2}{\mathrm{d}n} = -e^{-\beta n} \frac{f(n)}{\alpha - \beta} \,. \tag{41}$$

Differentiating (39) and using the boundary condition $T^{(2)}(0) = T_s^{(2)}$, we arrive at the following expression for the derivative at the surface

$$\frac{\mathrm{d}T_s^{(2)}}{\mathrm{d}n} = \alpha C_1(0) + \beta C_2(0) = \alpha T_s^{(2)} + C_2(0)(\beta - \alpha) \,. \tag{42}$$

In order to determine the value of $C_2(0)$ we integrate the second expression in (41). The constant of integration must be set to zero to prevent the exponential

growth of $T^{(2)}$ as $n \to \infty$:

$$C_2(0) = \frac{\mathcal{D}H^{(2)}}{\beta(\beta-\alpha)} + \frac{\alpha\left(T_\infty^{(0)} - T_s^{(0)}\right)}{(\beta-\alpha)^2} m_s^{(2)} + \frac{\mathcal{G}}{\beta-\alpha}\,, \quad \text{where} \tag{43}$$

$$\mathcal{G} = \frac{\alpha(T_\infty^{(0)} - T_s^{(0)})}{(\beta-\alpha)^2}\left(\alpha - \beta - m_s^{(0)}\right) + \frac{\alpha m_s^{(0)}}{\beta(\beta-\alpha)\rho_s}\left[1 - \mathcal{F}(0) + \frac{\beta}{\alpha}\left(1 - \frac{T_s^{(0)}}{T_\infty^{(0)}}\right)\log\frac{T_s^{(0)}}{T_\infty^{(0)}}\right], \tag{44}$$

and $\mathcal{F}(n) = {}_2\mathcal{H}_1\left[1;\, \beta/\alpha;\, (\alpha-\beta)/\alpha;\, (T_s^{(0)}/T_\infty^{(0)} - 1)e^{\alpha n}\right]$ is a hypergeometric function, while $H^{(2)}$ is defined by (36).

At this point we recall that the mass and heat fluxes at order κ must be matched to those on the solid-propellant side to satisfy the jump conditions given by (9). Rewritten for the gas-phase scales, (20) and (24) become

$$\frac{\mathrm{d}T^{(2)}(0)}{\mathrm{d}n} = T_s^{(2)} + \left[m_s^{(2)} - \lambda^*\right] T^* - m_s^{(2)} Q^*\,, \tag{45}$$

$$m_s^{(2)} = T_s^{(2)} m_s^{(0)}\left[\frac{1}{T^*+T_0} + \frac{Q^*\theta_s}{2(T^*+T_0)^2} - \frac{1}{2T^*-Q^*}\right] + \frac{\lambda^* T^*}{2T^*-Q^*}\,. \tag{46}$$

Here, as before, $T^* = T_s^{(0)} - T_0$, $Q^* = \tilde{Q}_s/\tilde{Q}_g$, and $\lambda^* = \tilde{\lambda}_s/\tilde{\lambda}_g$.

Substituting equations (43), (36), (45), and equation (46) into equation (42), we derive the curvature correction for the surface temperature as

$$\begin{aligned}
T_s^{(2)} &= A_1/A_2\,, \quad \text{where} \\
A_1 &= \left(1 + \frac{\mathcal{D}}{\beta m_s^{(0)}}\right)\left[a_1(T^*-Q^*) - \lambda^* T^*\right] + a_2 A_3 - \mathcal{G}\,, \\
A_2 &= \alpha + \frac{\mathcal{D}}{\beta} - m_s^{(0)} a_1 A_3 - \left(1 + \frac{\mathcal{D}}{\beta m_s^{(0)}}\right)\left[1 + m_s^{(0)} a_1\left(T_* - Q^*\right)\right], \\
A_3 &= \frac{\mathcal{D}(Q^*-T^*)}{\beta m_s^{(0)}} - \frac{\alpha(Q^*-T^*+1)}{\beta-\alpha}\,, \\
a_1 &= \frac{1}{2T^*-Q^*} - \frac{1}{T^*+T_0} - \frac{Q^*\theta_s}{2(T^*+T_0)^2}\,, \quad a_2 = \frac{\lambda^* T^*}{2T^*-Q^*}\,.
\end{aligned} \tag{47}$$

Having obtained the surface temperature correction, we can use (46) to derive an explicit form of the mass flux with curvature correction:

$$m_s = m_s^{(0)} + \kappa(a_1 m_s^{(0)} T_s^{(2)} + a_2) + O(\kappa^2)\,. \tag{48}$$

Therefore, the curvature correction to the regression rate of a weakly-curved EM deflagration front can be determined as follows. First, for given material properties, ambient pressure, and fresh mixture temperature T_0, the planar values of the mass flux and surface temperature are evaluated by solving (30)–(31). Next, for a given value of curvature κ, the surface temperature correction $T_s^{(2)}$ is calculated using (47). Finally, the mass flux is obtained through (48).

4 QUASISTEADY THEORY RESULTS

4.1 Verification of Solid Phase Asymptotics

To verify the above analysis, we solve the governing equations numerically and compare the asymptotic theory results with the numerical solutions in a simplified geometry. To estimate the accuracy of equation (22), we solve the heat equation in the solid phase of the burning spherical particle, or infinite cylinder, to find the burning rate as function of surface temperature.

We assume a quasi-steady burning regime, which sets the radius of the particle R to be constant. The spherical system of coordinates is set with the origin $r = 0$ at the center of the particle. The heat conservation equation for the incompressible conducting solid is written for the shifted coordinate $n = r - R$, so that $n = 0$ at the surface of the particle:

$$\frac{\mathrm{d}T}{\mathrm{d}n}\left[m - \frac{a}{(n+R)}\right] = \frac{\mathrm{d}^2T}{\mathrm{d}n^2} + \Omega_s\,, \tag{49}$$

$$T(0) = T_s\,, \quad T(-R) = T_0\,, \quad \frac{\mathrm{d}T(-R)}{\mathrm{d}n} = 0\,. \tag{50}$$

The third boundary condition in (50) reflects the assumption that the radius of the particle is much larger than the thermal penetration length. Parameter a is set equal to 1 in cylindrical geometry and to 2 in spherical geometry.

An iterative procedure finds the solution to (49) that satisfies boundary conditions (50), as well as the condition that the fuel has reacted completely as it leaves the solid phase domain. The surface temperature along with the fresh fuel temperature is preset, and the first guess for the mass flux is calculated using (22). One iterates on the temperature gradient at the interface until the boundary condition on temperature of the fresh fuel is satisfied. When this inner iteration loop is complete, the reaction source term is integrated over the entire computational domain using the obtained temperature profile to check if the complete reaction condition is satisfied. If not, a new guess for the mass flux is made. Hence, the outer iteration loop is on the mass flux, and the inner iteration loop is on the temperature gradient at the interface. Once iterations converge, one obtains the temperature profile that satisfies the heat equation with prescribed boundary conditions, as well as the condition of complete reaction.

The results of the simulation are compared to asymptotic formula (22) for HMX with $T_0 = 298$ K and $T_s = 750$ K in Fig. 2 (the material properties used for HMX in all the calculations presented in this paper can be found in Table 5.1). The curvature is negative for a particle, while positive curvature corresponds to a case when solid propellant surrounds a void, with the gaseous products of deflagration being removed from the center of the void (this last case is taken purely for purposes of the test, and can be viewed as a rough quasi-steady model for the combustion inside a large cavity with the radius much larger than the characteristic combustion-zone length). The planar regression rate value (at zero curvature) is in fair agreement with experimental data [27]

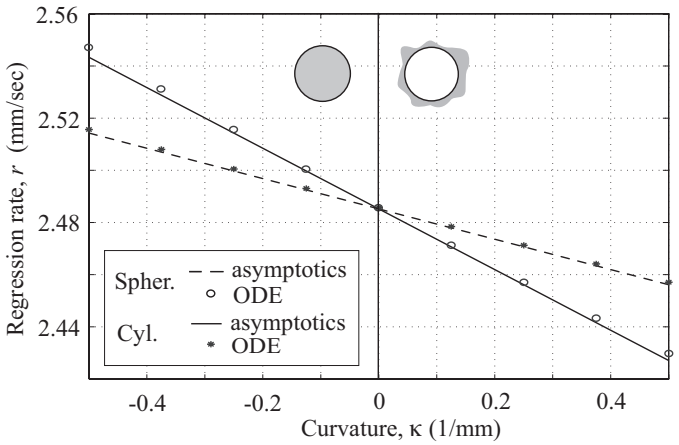

Figure 2: Regression rate of HMX as a function of surface curvature in spherical (solid line) and cylindrical (dashed line) geometry. The surface temperature is 750 K. Negative curvature corresponds to a burning particle/cylinder, while positive curvature corresponds to burning of a solid EM surrounding a cavity.

. As we expected, the line that is given by (22) is an asymptote to the ODE solution near zero curvature. For the values of T_s and T_0 that are picked for this calculation, the preheat length $l^* = \tilde{\lambda}_s/(\tilde{C}_p\tilde{m}_s)$ is equal to 31.9 μm. As the ratio of particle radius to preheat length becomes smaller, the ODE solution departs from the asymptote.

4.2 Verification of Burning Rate Curvature Correction Asymptotics

In the preceding section we have validated the asymptotic formula (22), and now we will apply it to solving the coupled solid–gas problem. To evaluate the accuracy of the asymptotic results, we solve the coupled problem of the particle deflagration numerically and obtain the mass flux as a function of particle radius, which is then compared with the result obtained from (47) and (48).

To calculate the curvature corrections, we first obtain the baseline value of the mass flux at the interface and the surface temperature from the solution of the planar problem. Such baseline value can be obtained in a number of ways, including the numerical solution of the planar deflagration problem or the method of matched asymptotics. We are going to employ the model presented in [11], where the solution of one-dimensional deflagration problem is reduced, in the limit of the small activation energy in the gas and high activation energy in the solid phase, to a set of algebraic equations. Following [11], we solve (30)–(31) to define baseline values for surface temperature and mass flux. Once base values are determined, we use (47) and (48) to determine the corrected values.

In the gas-phase, we numerically solve the problem formulated below. By

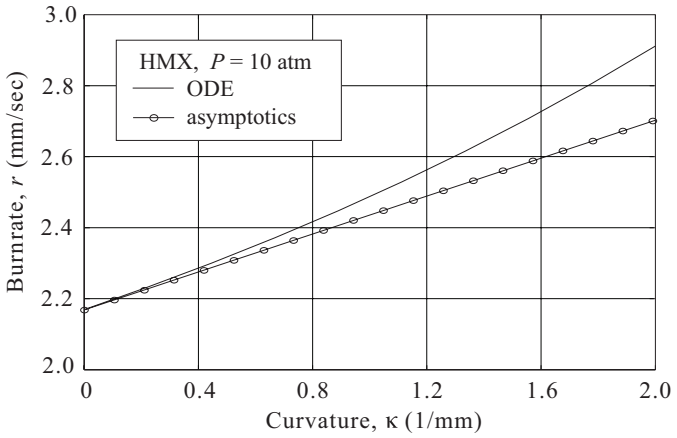

Figure 3: Burn rate of HMX at 10 atm, calculated by curvature asymptotics based on planar regression rate value calculated numerically, compared to burn rate calculated by solving coupled governing equations.

rewriting the heat and species conservation equations subject to boundary conditions $T(0) = T_s$, $T(\infty) = T_\infty$, $Y(\infty) = 0$ in spherical geometry for a special case of the unity Lewis number, we can employ the Shvab–Zel'dovich variables formulation, which gives the solution

$$T + Y = T_a + (T_\infty - T_a) \exp\left(-\frac{m_s R^2}{n + R}\right) , \tag{51}$$

where T_a is restricted by the boundary condition

$$T_a = T_s + 1 - \frac{1}{m_s} \frac{\mathrm{d}T(0)}{\mathrm{d}n} . \tag{52}$$

In this formulation, the heat equation is expressed in terms of temperature only. In the limit of a small activation energy, the heat equation becomes

$$\frac{\mathrm{d}^2 T}{\mathrm{d}n^2} + \frac{2(n + R) - m_s R^2}{(n + R)^2} \frac{\mathrm{d}T}{\mathrm{d}n} = \mathcal{D} \left[T - T_a - (T_\infty - T_a) \exp\left(-\frac{m_s R^2}{n + R}\right) \right] . \tag{53}$$

This equation has to be solved subject to boundary conditions $T(0) = T_s$, $T(\infty) = T_\infty$. Here n is the distance from the particle surface, R is the particle radius, m_s is the mass flux per unit area at the surface, and $\mathcal{D}$ is the Damkohler number.

The solution of the coupled solid–gas equation is obtained by iteration. In the solid phase, we solve (49). First an initial guess for surface temperature is made and iterations on the solid thermal structure are performed according to the scheme described previously. Next (53) is integrated with boundary conditions on surface temperature and mass flux obtained as a result of the

Table 1: Parameter Values Used for HMX [11]

$\tilde{\lambda}_s$	=	$0.2\,(W/mK)$	$\tilde{\lambda}_g$	=	$7.0 \times 10^{-2}\,(W/m\,K)$
$\tilde{\rho}_s$	=	$1800\,(kg/m^3)$	$\tilde{C}_p$	=	$1.4 \times 10^3\,(J/kg\,K)$
$\tilde{Q}_s$	=	$4.0 \times 10^5\,(J/kg)$	$\tilde{Q}_g$	=	$3018 \times 10^3\,(J/kg)$
$\tilde{B}$	=	$1.6 \times 10^{-3}\,(m^3/kg\,s\,K^2)$	$\tilde{\mathcal{M}}_g$	=	$34.2 \times 10^{-3}\,(kg/mole)$
$\tilde{Z}$	=	$1.63 \times 10^{15}\,(1/s)$	$\tilde{E}_s$	=	$1.76 \times 10^5\,(J/mole)$

solid-phase iterations. The heat fluxes on both sides of the interface are then compared and the outer iteration loop is repeated by adjusting the surface temperature until the heat flux is continuous across the interface.

Figure 3 presents the result of asymptotics validation test for a material with properties modeled after HMX. The ambient pressure value is taken to be equal to 10 atm. The burn rate calculated by curvature asymptotics is compared to the burn rate calculated by solving coupled governing equations. The planar regression rate value was obtained numerically and kept the same for both calculations. For small values of curvature the results are almost identical, while as the curvature becomes larger, the asymptotic value becomes less accurate.

5 UNSTEADY DEFLAGRATION

5.1 Formulation

To complete our quasi-steady model study, we show that the quasi-steady approach is indeed appropriate for the mass-flux eigenvalue calculation. This additional verification step involves numerically solving a full set of the unsteady equations describing deflagration of a spherical EM particle and comparing the results with those obtained within the framework of the quasi-steady theory.

A numerical procedure for representing the motion of the interface has to be identified to solve the unsteady problem. A relatively simple approach that can produce an explicit regression rate formula is to represent the chemical reaction in the solid phase by a jump in the heat flux across the material interface. In [16], such an approach was used together with the pyrolysis law to define the regression rate of a burning propellant surface. Unfortunately, we may not use such an approach. Given our modeling assumptions we must resolve a thin reaction layer in the solid phase and obtain the burning rate as an eigenvalue. Also, since the pyrolysis law does not reflect the curvature dependence of the regression rate, prescribing the regression rate law as in [16] would undermine the purpose of the numerical experiment. To achieve our modeling goal we follow [28] and introduce an additional reactant conservation equation in the solid phase. The imposition of an additional boundary condition of full reactant consumption at the interface allows us to determine the interface regression velocity.

The governing equations are written in the frame attached to the regressing

surface. The choice of frame of reference attached to the interface over the laboratory frame of reference was the result of an extensive study of algorithms currently used for simulating problems that involve moving material interfaces and is discussed in Appendix 9.

In the gas phase, we solve

$$\frac{\partial \rho}{\partial t} + \frac{\partial (\rho U_n)}{\partial n} + 2\rho \frac{U_n + D}{R+n} = 0\,, \tag{54}$$

$$\frac{\partial (\rho U_n)}{\partial t} + \rho \frac{\partial D}{\partial t} + \frac{\partial (\rho U_n^2)}{\partial n} =$$

$$-\frac{\partial p_1}{\partial n} + Pr^* \left[\frac{\partial^2 U_n}{\partial n^2} + \frac{2}{R+n} \frac{\partial U_n}{\partial n} \right] + Pr^* \frac{2(U_n + D)}{(R+n)^2}\,, \tag{55}$$

$$\rho \left(\frac{\partial T}{\partial t} + U_n \frac{\partial T}{\partial n} \right) = \frac{\partial^2 T}{\partial n^2} + \frac{2}{R+n} \frac{\partial T}{\partial n} + \mathcal{D} Y\,, \tag{56}$$

$$\frac{\partial Y}{\partial t} + U_n \frac{\partial Y}{\partial n} = \frac{\partial^2 Y}{\partial n^2} + \frac{2}{R+n} \frac{\partial Y}{\partial n} - \mathcal{D} Y\,, \tag{57}$$

$$\rho T = 1\,. \tag{58}$$

In the solid phase,

$$\frac{\partial T}{\partial t} + a_1 \frac{\partial T}{\partial n} = a_2 \left(\frac{\partial^2 T}{\partial n^2} + \frac{2}{R+n} \frac{\partial T}{\partial n} \right) + a_3 \frac{\tilde{Q}_c}{\tilde{Q}_g} \exp\left(-\frac{a_4}{T} \right)\,, \tag{59}$$

$$\frac{\partial Y_c}{\partial t} + a_1 \frac{\partial Y_c}{\partial n} = -a_3 \exp\left(-\frac{a_4}{T} \right)\,. \tag{60}$$

In the analysis part of the paper, we used different scaling in the gas and solid phase for clarity of representation, and kept track of this difference while applying the boundary conditions at the interface. In the numerical simulation, the scaling is based on the gas phase characteristic values for both gas and solid phases, so that gas phase equations take conventional scaled form, while certain terms in the solid phase governing equations pick up additional dimensionless multipliers defined as

$$a_1 = \frac{\tilde{C}_p \tilde{D} \tilde{P} \tilde{\mathcal{M}}}{\tilde{m}_c \tilde{Q}_g \tilde{\mathcal{R}}}\,, \quad a_2 = \frac{\tilde{C}_p \tilde{P} \tilde{\mathcal{M}} \tilde{\lambda}_c}{\tilde{Q}_g \tilde{\mathcal{R}} \tilde{\lambda}_g \tilde{\rho}_c}\,, \quad a_3 = \frac{\tilde{A}_s \tilde{P} \tilde{\mathcal{M}} \tilde{\lambda}_g}{\tilde{m}_c^2 \tilde{Q}_g \tilde{\mathcal{R}}}\,, \quad a_4 = \frac{\tilde{C}_p \tilde{E}_s}{\tilde{Q}_g \tilde{\mathcal{R}}}\,. \tag{61}$$

The connection conditions require that mass, momentum and energy be conserved across the interface, the net flux of gas phase reactant at the interface is equal to unity and all the condensed phase reactant is consumed by the time material particles reach the interface:

$$[m] = 0\,, \quad [T] = 0\,, \tag{62}$$

$$\left[\tilde{\lambda} \frac{\partial T}{\partial n} \right] = 0\,, \quad Y(0,t) - \frac{1}{m_s} \frac{\partial Y(0,t)}{\partial n} = 1\,, \quad Y_s(0,t) = 0\,. \tag{63}$$

In spherical geometry, when ambient temperature is not equal to the adiabatic flame temperature, there exists an additional length scale that we need to

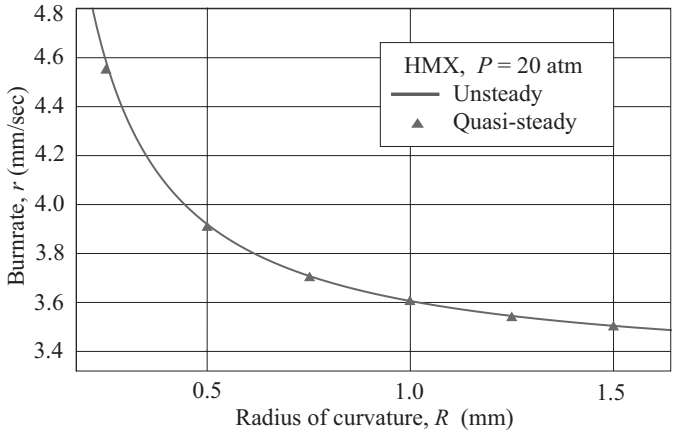

Figure 4: Burn rate as function of particle radius calculated in the unsteady simulation of particle deflagration (solid line) compared with those calculated in quasi-steady regime.

consider: the thermal relaxation scale which is generally much larger than the reaction scale in the gas phase. To resolve both relatively short reaction scale and long conduction scale, we introduce a coordinate transformation ($n \to y$) such that

$$\text{for } n > 0\,, \quad y = \log(1+n)\,; \quad \text{for } n < 0\,, \quad y = -\log(1-n)\,. \tag{64}$$

The coupled solid–gas system of equations is solved using a semi-implicit finite difference method suggested in [29]. The scheme uses second order central differences on a staggered grid, with a predictor-corrector time update. At $t = 0$, a steady state solution is used as the initial condition. Next the connection conditions at the interface are applied to determine surface temperature T_s and regression velocity D. The predictor step is made and T_s, D are updated from predicted field variables. Then the corrector step follows. The above sequence is repeated until simulation end time is reached. Accuracy of current scheme was verified as second order globally and first order at the interface.

Results of the simulation are presented on Fig. 4. An HMX particle with initial diameter of 2×10^{-3} m is burnt in an inert atmosphere with the ambient pressure equal to 20 atm. The planar steady deflagration profiles are given as initial conditions. After the initial transient, a new quasi-steady burning regime is attained, and the burning rate is tracked as a function of the particle radius R. The final particle size is size is 2×10^{-4} m, which is still larger than the preheat length for the given ambient pressure value. The experiment is then repeated for a set of fixed particle radii, to obtain the quasi-steady regression rate as a function of the particle radius. When the values of the regression rate from unsteady experiment are compared to those in the quasi-steady framework, a satisfactory agreement is observed.

6 CONCLUSIONS

In the limit of small curvature, we derived a set of conservation equations with a curvature correction for deflagration of a solid homogeneous EM. By using the method of matched asymptotics we obtained the mass flux across a curved burning surface as the solid phase heat equation eigenvalue.

The coupled set of governing equations for gas and solid phases was solved to reveal an explicit form of the first curvature corrections for the mass flux at the surface and the surface temperature, as functions of the boundary conditions and material parameters.

These results were compared with numerical solution of the corresponding test problems. The comparison revealed good agreement for the values of curvature and boundary conditions that preserve the assumption of curvature smallness relative to the inverse preheat zone thickness. We conclude that the question posed in the introduction section of this paper, whether the curvature correction is significant or not, has a positive answer: yes, it can be significant. At certain values of the ambient pressure and curvature, such correction can be as large as 10% and more. As an illustration, we studied the deflagration of a sphere in an inert atmosphere under the assumptions of the current model.

Finally, we performed a check of the quasi-steady assumption that was used to model EM deflagration, by comparing the results obtained under that assumption with those obtained from the fully-coupled unsteady simulation of a spherical particle deflagration. The comparison revealed that the quasi-steady models can indeed accurately predict the burn rates of the solid propellant as long as the premise of the curvature smallness is held.

Application of the current asymptotic result to the existing solid propellant deflagration models is straightforward. Immediate benefit can be obtained from application of this result to large scale multi-dimensional solid-propellant deflagration simulations. Derivation of the curvature correction does not require any particular way of determining the baseline planar values of surface temperature and mass flux. Therefore, any methods currently used in existing models (such as pressure power law, pyrolysis, etc.) can be preserved without any modification. The curvature correction can be calculated post facto and used to modify the planar value.

Future studies of the influence of curvature effects on flame stability are warranted. Also, a more comprehensive model of the solid phase needs to be investigated in order to evaluate the combined effects of curvature and thermoelasticity.

ACKNOWLEDGEMENTS

The University of Illinois Center for Simulation of Advanced Rockets research program is supported by the US Department of Energy through the University of California under sub contract B341494. D. S. Stewart has also been supported by the Los Alamos National Laboratory, DOE/LANL I2933-0019 and the US

Air Force.

References

[1] Landau L.D. and E.M Lifshiz. *Fluid Mechanics*. Butterworth-Heinemann, Oxford, 2000.

[2] Drozdov P. G. and Y .B. Zeldovich. Diffusion phenomena near the limit of propagation of flame. experimental study of the detonation of explosive mixtures of carbon monoxide. *J. Phys. Chem. (USSR)*, 17, 1943.

[3] Matalon M. and B.J. Matkowsky. Flames as gasdynamic discontinuities. *Journal of Fluid Mechanics*, 124:239–259, 1982.

[4] Yao J. and D.S. Stewart. On the dynamics of multi-dimensional detonation. *Journal of Fluid Mechanics*, 309:225–275, 1996.

[5] Chorpening B. T., Knott G. M., and M. Q. Brewster. Flame structure and burning rate of AP/HTPB propellant sandwiches. In *Proceedings of The Combustion Institute*, volume 28:1, pages 847–853. Combustion Institute, 2000.

[6] Massa L., Jackson T.L., and M. Short. Numerical solution of three-dimensional heterogeneous solid propellants. *Combustion Theory and Modelling*, 7:579–602, 2003.

[7] Zel'dovich Ya. B. On the theory of combustion of powders and explosives. *Zurnal Experimental'noi i Teoreticheskoi Fisiki*, 12(11–12):498–524, 1942.

[8] Merzhanov A. G. and F. I. Dubovitskii. The theory of stationary combustion in powders. *Proc. USSR Acad. Sci.*, 129:153–156, 1959.

[9] Lengelle G. Thermal degradation kinetics and surface pyrolysis of vinyl polymers. *AIAA Journal*, 8:1989–1998, 1970.

[10] Margolis S.B. and F.A. Williams. Structure and stability of deflagrations in porous energetic materials. In *Progress in Astronautics and Aeronautics*, volume 185, pages 549–590. AIAA Inc., 2000.

[11] Ward M.J., Son S.F., and M.Q. Brewster. Role of gas- and condensed-phase kinetics in burning rate control of energetic solids. *Combustion Theory and Modelling*, 2:293–312, 1998.

[12] Kuznetsov I.R. and D.S. Stewart. Burning rate of homogeneous energetic materials with thermal expansion and varying thermal properties in the condensed phase. *CombustionTheory and Modelling*, 9(2):255–272, 2005.

[13] Davidson J.E. and M.W. Beckstead. A three-phase model of HMX combustion. In *Proceedings of the Twenty-Sixths Symposium (International) on Combustion*, pages 1989–1996. Combustion Institute, 1996.

[14] Prasad K., Yetter R.A., and M. D. Smooke. An eigenvalue method for coupling the burning rates of HMX propellants. *Combustion and Flame Journal*, 115:406–416, 1998.

[15] Liau Y., Yang V., and S.T. Thynell. Modeling of RDX/GAP propellant combustion with detailed chemical kinetics. In *Progress in Astronautics and Aeronautics*, volume 185, pages 477–500. AIAA Inc., 2000.

[16] Wang X., Jackson T.L., and L. Massa. Numerical simulation of heterogeneous propellant combustion by a level set method. *Combustion Theory and Modelling*, 8:227–254, 2004.

[17] Yoon J.-K., Thakre P., and V. Yang. Modeling of RDX/GAP/BTTN pseudo-propellant combustion. *Combustion and Flame Journal*, 145(1–2):300–315, 2006.

[18] Williams F. A. *Combustion Theory*, pages 238–243. Addison-Wesley, New York, 2nd edition, 1985.

[19] Fendell F.E. Asymptotic analysis of premixed burning with large activation energy. *Journal of Fluid Mechanics*, 56:81—95, 1972.

[20] Ludford G.S.S., Yannitell D.W., and J.D. Buckmaster. The decomposition of a cold monopropellant in an inert atmosphere. *Combustion Science and Technology*, 14:133–146, 1976.

[21] Fendell F.E. Quasi-steady sphericosymmetric monopropellant decomposition in inert and reactive environments. *Combustion Science and Technology*, 1:131–145, 1969.

[22] Zenin A.A. HMX and RDX: Combustion mechanism and influence on modern double-base propellant combustion. *Journal of Propulsion and Power*, 11:752–758, 1995.

[23] Stewart D.S. and J.B. Bdzil. The shock dynamics of stable multidimensional detonation. *Combustion and Flame*, 72:311–323, 1988.

[24] Buckmaster J. D. and G. S. S. Ludford. *Theory of Laminar Flames*. Cambridge University Press, 1982.

[25] Kuznetsov I.R. *Modeling the Thermo-Mechanical Structure of Energetic Material Flames*. PhD thesis, UIUC, 2005.

[26] A. F Filippov. *Problems in differential equations*. W. H. Freeman, 1966.

[27] Lengelle G., Duterque J., and F. Trubert. Physico-chemical mechanisms of solid propellant combustion. In *Progress in Astronautics and Aeronautics*, volume 185, pages 287–334. AIAA Inc., 2000.

[28] Jackson T.L., Massa L., and M.Q. Brewster. Unsteady combustion modelling of energetic solids, revisited. *Combustion Theory and Modelling*, 8:513–532, 2004.

[29] Najm H.N., Wyckoff P.S., and O.M. Knio. A semi-implicit numerical scheme for reacting flow. *Journal of Computational Physics*, 143:381–402, 1998.

[30] Shyy W., Udaykumar H. S., Rao M. M., and R. W. Smith. *Computational fluid dynamics with moving boundaries*. Taylor and Francis, London, 1996.

[31] Zhao P.H. and J.C. Heinrich. Approximation to the interface velocity in phase change front tracking. *Communications in numerical methods in engineering*, 18:77–88, 2002.

7 Governing equations in Betrand-intrinsic coordinates.

The presentation of Betrand-intrinsic coordinates formalism in this Appendix closely follows that in [4]. The coordinate transformation between the laboratory frame of reference and the intrinsic coordinates frame of reference is defined as

$$\vec{x} = \vec{x_s}(\xi, t) + n\hat{n}(\xi, t), \quad \vec{v} = v_\xi \hat{t} + v_n \hat{n}\,,$$

with local orthogonality of the coordinate system indicated by Frenet formulae, which in two dimensions are

$$\frac{\partial \hat{t}}{\partial \xi} = -\kappa \hat{n}\,, \quad \frac{\partial \hat{n}}{\partial \xi} = \kappa \hat{t}\,.$$

We define the normal component of the interface velocity as $D_n \equiv -\left(\partial n/\partial t\right)_{\vec{x}}$, and instantaneous surface stretch as $B \equiv \left(\partial \xi/\partial t\right)_{\vec{x}}$, evaluated at $n = 0$. Then, the time derivatives in the two frames of reference are related by

$$\left(\frac{\partial}{\partial t}\right)_{\vec{x}} = \left(\frac{\partial}{\partial t}\right)_{\vec{\xi}} - D_n \frac{\partial}{\partial n} + B\frac{\partial}{\partial \xi}\,.$$

Now we can calculate the following useful vector algebra identities in the intrinsic coordinates

$$\left(\frac{\partial \hat{n}}{\partial t}\right)_{\vec{\xi}} = -\left(\frac{\partial D}{\partial \xi} + B\kappa\right)\hat{t}\,, \quad \left(\frac{\partial \hat{t}}{\partial t}\right)_{\vec{\xi}} = \left(\frac{\partial D}{\partial \xi} + B\kappa\right)\hat{n}\,,$$
$$\frac{\partial D}{\partial n} = \frac{\partial \kappa}{\partial n} = \frac{\partial n}{\partial \xi} = \frac{\partial \hat{t}}{\partial n} = \frac{\partial \hat{n}}{\partial n} = 0\,.$$

These identities are used to rewrite the combustion approximation equations as follows. The continuity equation becomes

$$\frac{\partial \rho}{\partial t} + \frac{\partial(\rho U_n)}{\partial n} + \kappa\frac{\rho(U_n + D_n)}{(1+n\kappa)} + \frac{1}{(1+n\kappa)}\frac{\partial(\rho v_\xi)}{\partial \xi} + B\frac{\partial \rho}{\partial \xi} = 0\,.$$

The momentum equation in n is recast as

$$\frac{\partial U_n}{\partial t} + \frac{\partial D}{\partial t} + U_n\frac{\partial U_n}{\partial n} + \frac{1}{\rho}\frac{\partial p_1}{\partial n} + \left(\frac{v_\xi}{1+n\kappa} + B\right)\frac{\partial v_n}{\partial \xi} - v_\xi^2\frac{\kappa}{(1+n\kappa)} + v_\xi\frac{\partial D}{\partial \xi}$$
$$-\frac{Pr}{\rho}\left[\frac{\partial^2 v_n}{\partial n^2} + \frac{\kappa}{1+n\kappa}\frac{\partial v_n}{\partial n} + \frac{1}{(1+n\kappa)^2}\left(\frac{\partial^2 v_n}{\partial \xi^2} - v_n\kappa^2 - 2\kappa\frac{\partial v_\xi}{\partial \xi} - v_\xi\frac{\partial \kappa}{\partial \xi}\right)\right]$$
$$-\frac{Pr}{\rho}\frac{n}{(1+n\kappa)^3}\frac{\partial \kappa}{\partial \xi}\left(\frac{\partial v_n}{\partial \xi} - v_\xi\kappa\right)$$
$$-\frac{Pr_\nu}{\rho}\left[\frac{\partial^2 v_n}{\partial n^2} - \frac{\kappa}{(1+n\kappa)^2}\left(\kappa v_n + \frac{\partial v_\xi}{\partial \xi}\right) + \frac{1}{1+n\kappa}\left(\frac{\partial v_n}{\partial n}\kappa + \frac{\partial^2 v_\xi}{\partial \xi \partial n}\right)\right] = 0\,.$$

Momentum in ξ:

$$\frac{\partial v_\xi}{\partial t} + U_n \frac{\partial v_\xi}{\partial n} + \frac{1}{\rho(1+n\kappa)} \frac{\partial p_1}{\partial \xi} + \left(\frac{v_\xi}{1+n\kappa} + B \right) \frac{\partial v_\xi}{\partial \xi} + v_n v_\xi \frac{\kappa}{1+n\kappa} - v_n \frac{\partial D}{\partial \xi}$$
$$- \frac{Pr}{\rho} \left[\frac{\partial^2 v_\xi}{\partial n^2} + \frac{\kappa}{1+n\kappa} \frac{\partial v_\xi}{\partial \xi} + \frac{1}{(1+n\kappa)^2} \left(\frac{\partial^2 v_\xi}{\partial \xi^2} - v_\xi \kappa^2 + 2\kappa \frac{\partial v_n}{\partial \xi} + v_n \frac{\partial \kappa}{\partial \xi} \right) \right]$$
$$- \frac{Pr_\nu}{\rho(1+n\kappa)} \left[\frac{\partial^2 v_n}{\partial \xi \partial n} - \frac{n}{(1+n\kappa)^2} \frac{\partial \kappa}{\partial \xi} \left(\kappa v_n + \frac{\partial v_\xi}{\partial \xi} \right) \right]$$
$$- \frac{n}{(1+n\kappa)^3} \frac{\partial \kappa}{\partial \xi} \left(\frac{\partial v_\xi}{\partial \xi} + v_n \kappa \right) - \frac{Pr_\nu}{\rho(1+n\kappa)^2} \left(\frac{\partial \kappa}{\partial \xi} v_n + \frac{\partial v_n}{\partial \xi} \kappa + \frac{\partial^2 v_\xi}{\partial \xi^2} \right) = 0 \,.$$

Energy:

$$\rho \frac{\partial T}{\partial t} + \rho U_n \frac{\partial T}{\partial n} + \rho \frac{\partial T}{\partial \xi} \left(\frac{v_\xi}{1+n\kappa} + B \right) - \frac{\partial^2 T}{\partial n^2} - \frac{1}{(1+n\kappa)^2} \frac{\partial^2 T}{\partial \xi^2}$$
$$- \frac{\kappa}{1+n\kappa} \frac{\partial T}{\partial n} + \frac{n}{(1+n\kappa)^3} \frac{\partial \kappa}{\partial \xi} \frac{\partial T}{\partial \xi} - \Omega_g = 0 \,.$$

Species:

$$Le \left[\rho \frac{\partial Y}{\partial t} + \rho U_n \frac{\partial Y}{\partial n} + \rho \frac{\partial Y}{\partial \xi} \left(\frac{v_\xi}{1+n\kappa} + B \right) \right] - \frac{\partial^2 Y}{\partial n^2} - \frac{1}{(1+n\kappa)^2} \frac{\partial^2 Y}{\partial \xi^2}$$
$$- \frac{\kappa}{1+n\kappa} \frac{\partial Y}{\partial n} + \frac{n}{(1+n\kappa)^3} \frac{\partial \kappa}{\partial \xi} \frac{\partial Y}{\partial \xi} + Le\, \Omega_g = 0 \,.$$

Analogously, we rewrite the solid phase energy conservation equation:

$$\rho \frac{\partial T}{\partial t} + \rho U_n \frac{\partial T}{\partial n} + \rho \frac{\partial T}{\partial \xi} \left(\frac{v_\xi}{1+n\kappa} + B \right) - \frac{\partial^2 T}{\partial n^2} - \frac{1}{(1+n\kappa)^2} \frac{\partial^2 T}{\partial \xi^2}$$
$$- \frac{\kappa}{1+n\kappa} \frac{\partial T}{\partial n} + \frac{n}{(1+n\kappa)^3} \frac{\partial \kappa}{\partial \xi} \frac{\partial T}{\partial \xi} + \Omega_s = 0 \,.$$

8 Formal expansion in powers of curvature.

The reduced governing equations presented in Appendix 7 are valid in the asymptotic sense close to the interface, where $n = O(1)$. We also require that the dimensionless surface curvature be small.

We take a small parameter ϵ^2 to be a measure of magnitude of the curvature, so that $\kappa = \epsilon^2 \hat{\kappa}$, where $0 < \epsilon << 1$ and $\hat{\kappa} = O(1)$. Variation of the flow structure in the transverse direction is assumed to be weak, and is characterized by transverse scaled variable $\zeta = \epsilon \xi = O(1)$. The interface velocity scales as $D = O(1)$, and the interface stretch has the magnitude $B = O(\epsilon)$.

Based on these assumptions, we are looking for asymptotic expansions of the dependent variables in the following form:

$$U_n \;\; = \;\; U_n^{(0)} + \epsilon^2 U_n^{(2)} + \dots \,,$$

$$
\begin{aligned}
v_\xi &= \epsilon v_\xi^{(1)} + \epsilon^2 v_\xi^{(2)} + \dots , \\
\rho &= \rho^{(0)} + \epsilon^2 \rho^{(2)} + \dots , \\
p_1 &= p_1^{(0)} + \epsilon^2 p_1^{(2)} + \dots , \\
Y &= Y^{(0)} + \epsilon^2 Y^{(2)} + \dots , \\
T &= T^{(0)} + \epsilon^2 T^{(2)} + \dots , \\
D &= D^{(0)} + \epsilon^2 D^{(2)} + \dots , \\
B &= \epsilon B^{(1)} + \epsilon^2 B^{(2)} + \dots ,
\end{aligned}
$$

with $v_n^{(i)} = U_n^{(i)} + D^{(i)}$. Substituting these expansions into the scaled governing equations in the intrinsic coordinates (Appendix 7) and collecting terms at the first three orders $O(1)$, $O(\epsilon)$ and $O(\epsilon^2)$, for the gas phase at $O(1)$ we obtain:

$$
\begin{aligned}
\frac{\partial}{\partial n}(\rho^{(0)} U_n^{(0)}) &= 0 , \\
U_n^{(0)} \frac{\partial U_n^{(0)}}{\partial n} + \frac{1}{\rho} \frac{\partial p_1^{(0)}}{\partial n} - \frac{(Pr + Pr_\nu)}{\rho^{(0)}} \frac{\partial^2 U_n^{(0)}}{\partial n^2} &= 0 , \\
0 &= 0 , \\
\rho^{(0)} U^{(0)} \frac{\partial T^{(0)}}{\partial n} - \frac{\partial^2 T^{(0)}}{\partial n^2} - \Omega_g^{(0)} &= 0 , \\
\rho^{(0)} U^{(0)} \frac{\partial Y^{(0)}}{\partial n} - \frac{1}{Le} \frac{\partial^2 Y^{(0)}}{\partial n^2} + \Omega_g^{(0)} &= 0 .
\end{aligned}
$$

At $O(\epsilon)$:

$$
\{0\} = \{0\} .
$$

At $O(\epsilon^2)$:

$$
\begin{aligned}
\frac{\partial}{\partial n}(\rho^{(2)} U_n^{(0)} + \rho^{(0)} U_n^{(2)}) + \hat{\kappa} \rho^{(0)} \left(U_n^{(0)} + D^{(0)} \right) &= 0 , \\
\rho^{(0)} U_n^{(0)} \frac{\partial U_n^{(2)}}{\partial n} + \rho^{(0)} U_n^{(2)} \frac{\partial U_n^{(0)}}{\partial n} + \rho^{(2)} U_n^{(0)} \frac{\partial U_n^{(0)}}{\partial n} + \frac{\partial p_1^{(2)}}{\partial n} & \\
-(Pr + Pr_\nu) \left(\frac{\partial^2 U_n^{(2)}}{\partial n^2} + \hat{\kappa} \frac{\partial U_n^{(0)}}{\partial n} \right) &= 0 , \\
\rho^{(0)} U_n^{(0)} \frac{\partial v_\xi^{(2)}}{\partial n} - Pr \frac{\partial^2 v_\xi^{(2)}}{\partial n^2} &= 0 , \\
\rho^{(0)} U^{(0)} \frac{\partial T^{(2)}}{\partial n} + \rho^{(0)} U^{(2)} \frac{\partial T^{(0)}}{\partial n} + \rho^{(2)} U^{(0)} \frac{\partial T^{(0)}}{\partial n} & \\
- \frac{\partial^2 T^{(2)}}{\partial n^2} - \hat{\kappa} \frac{\partial T^{(0)}}{\partial n} - \Omega_g^{(2)} &= 0 , \\
\rho^{(0)} U^{(0)} \frac{\partial Y^{(2)}}{\partial n} + \rho^{(0)} U^{(2)} \frac{\partial Y^{(0)}}{\partial n} + \rho^{(2)} U^{(0)} \frac{\partial Y^{(0)}}{\partial n} & \\
- \frac{1}{Le} \left(\frac{\partial^2 Y^{(2)}}{\partial n^2} + \hat{\kappa} \frac{\partial Y^{(0)}}{\partial n} \right) + \Omega_g^{(2)} &= 0 .
\end{aligned}
$$

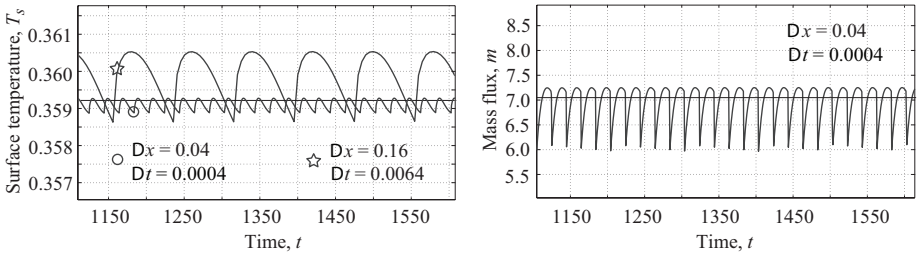

Figure 5: Planar deflagration values by interface tracking (oscillatory profiles) and from the solution of steady equations in the frame of reference attached to the solid-gas interface (straight line). Left: the amplitude of the surface temperature oscillations can be reduced sufficiently (0.15% of the steady-state value) as the resolution is increased. Right: the amplitude of the mass flux oscillations remains significant (17% of the steady-state value) even at high resolution.

For the solid phase, at $O(1)$:

$$\rho^{(0)} U^{(0)} \frac{\partial T^{(0)}}{\partial n} = \frac{\partial^2 T^{(0)}}{\partial n^2} + \Omega_s^{(0)} \,,$$

At $O(\epsilon)$:

$$\{0\} = \{0\} \,,$$

At $O(\epsilon^2)$:

$$\rho^{(0)} U^{(0)} \frac{\partial T^{(2)}}{\partial n} + \rho^{(0)} U^{(2)} \frac{\partial T^{(0)}}{\partial n} + \rho^{(2)} U^{(0)} \frac{\partial T^{(0)}}{\partial n} - \frac{\partial T^{(0)}}{\partial n} \hat{\kappa} = \frac{\partial^2 T^{(2)}}{\partial n^2} + \Omega_s^{(2)} \,.$$

9 Moving interface algorithms

There are conceptual advantages to using the laboratory frame of reference when solving problems with coupled interfaces, specifically if one considers the interface tracking that allows representation of arbitrary multi-dimensional shapes and surfaces. Moreover, an interface tracking algorithm, in combination with the level set method, has been implemented recently for multimaterial simulation of heterogeneous solid propellant deflagration [16].

We have attempted to implement interface tracking for one-dimensional deflagration model (54-60) rewritten in the laboratory frame, where the interface position at each time step was computed based on regression rate velocity at previous time steps. It was observed that, regardless of the discretization algorithm, the values of field variables oscillate near the interface as it moves between grid points, with a period of oscillation equal to time needed to traverse one grid cell. Similar to what is reported in [16], we found that the oscillations diminish with increased spatial resolution (Fig. 5).

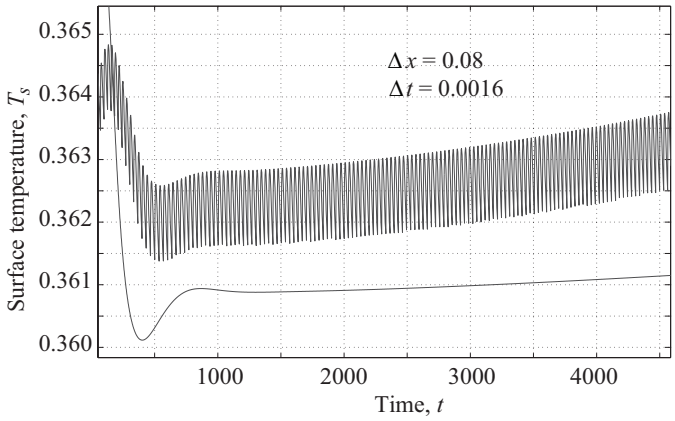

Figure 6: Burn rate of an HMX particle with initial radius of 10^{-3} m at 20 atm as a function of particle radius. The results by two algorithms are shown: the highly oscillatory profile from the simulation with interface tracking, and the lower, non-oscillatory profile from the simulation in a frame of reference attached to the solid-gas interface.

Even though the amplitude of oscillation of some field variables (such as temperature) can be reduced significantly at the cost of higher spatial resolution, the amplitude of interface velocity oscillations remains quite large. For planar deflagration of HMX at 20 atm (Figure 5), the interface temperature oscillations within only 0.15% of the steady-state value produce oscillations in mass flux across the interface with the amplitude of around 17% of the steady-state value. The reason for such sensitive behavior is clear since the activation energy of the solid phase chemical reaction is often high, which means that even a small change in the surface temperature leads to a significant change in the reaction rate and hence in the interface velocity.

A fully coupled deflagration problem was simulated in planar and spherical geometry in both laboratory frame system of coordinates with interface tracking, and in a system of coordinates attached to the moving deflagration front, when the grid is moving in the laboratory frame together with the interface. A comparison of interface temperature evolution in time for burning in spherical geometry showed that, even though moving interface algorithm produces qualitatively correct results (Fig. 6) — as the radius of particle decreases, the surface temperature is increased — the rate at which such increase occurs is different from that obtained by a more accurate algorithm that solves governing equations in a system of coordinates travelling with the interface.

A study of interface-tracking algorithms and the inherent oscillations near the solid–gas interface that such algorithms produce was performed. It was concluded, based on the existing reports and studies of such oscillations [16, 30, 31] and our experience, that interface-tracking algorithms on the fixed grid are suitable for modeling the EM deflagration when it is possible to reduce

the amplitude of surface velocity oscillations by simple grid refinement, without exceeding the limits of computability of the problem at hand. In case when the mass flux, or the regression rate depends on the high activation energy kinetics in the solid phase, the value of the mass flux is highly sensitive to even relatively small oscillations of the surface temperature. If one's goal is to capture curvature correction effects by evaluating a relatively small changes in mass flux and surface temperature related to curvature, a systematic error that may well be of the same order of magnitude as the effects of interest is not acceptable. Therefore we restricted our formulation to coordinates attached to the interface to obtain the desired accuracy, and recommend that the use of interface tracking methods on the fixed grid be avoided, unless an effective oscillation-suppressing algorithm is available.